

Momentum-Resolved Electronic Structure of the High- T_c Superconductor Parent Compound BaBiO_3

N. C. Plumb,^{1,*} D. J. Gawryluk,^{2,†} Y. Wang,³ Z. Ristić,¹ J. Park,¹ B. Q. Lv,^{4,1} Z. Wang,^{1,5}
C. E. Matt,¹ N. Xu,¹ T. Shang,² K. Conder,² J. Mesot,^{6,7,8} S. Johnston,³ M. Shi,¹ and M. Radović^{1,9}

¹Swiss Light Source, Paul Scherrer Institut, CH-5232 Villigen PSI, Switzerland

²Laboratory for Scientific Developments and Novel Materials,
Paul Scherrer Institut, CH-5232 Villigen PSI, Switzerland

³Department of Physics and Astronomy, University of Tennessee, Knoxville, Tennessee 37996-1200, USA

⁴Beijing National Laboratory for Condensed Matter Physics and Institute of Physics,
Chinese Academy of Sciences, Beijing 100190, China

⁵Department of Quantum Matter Physics, 24 Quai Ernest-Ansermet, 1211 Geneva 4, Switzerland

⁶Paul Scherrer Institut, CH-5232 Villigen PSI, Switzerland

⁷Institute of Condensed Matter Physics, École Polytechnique Fédérale de Lausanne (EPFL), CH-1015 Lausanne, Switzerland

⁸Laboratory for Solid State Physics, ETH Zürich, CH-8093 Zürich, Switzerland

⁹SwissFEL, Paul Scherrer Institut, CH-5232 Villigen PSI, Switzerland

(Dated: September 17, 2018)

We investigate the band structure of BaBiO_3 , an insulating parent compound of doped high- T_c superconductors, using *in situ* angle-resolved photoemission spectroscopy on thin films. The data compare favorably overall with density functional theory calculations within the local density approximation, demonstrating that electron correlations are weak. The bands exhibit Brillouin zone folding consistent with known BiO_6 breathing distortions. Though the distortions are often thought to coincide with $\text{Bi}^{3+}/\text{Bi}^{5+}$ charge ordering, core level spectra show that bismuth is monovalent. We further demonstrate that the bands closest to the Fermi level are primarily oxygen derived, while the bismuth $6s$ states mostly contribute to dispersive bands at deeper binding energy. The results support a model of Bi-O charge transfer in which hole pairs are localized on combinations of the O $2p$ orbitals.

PACS numbers: 74.20.Pq, 74.25.Jb, 74.70.-b, 71.20.Nr

A central challenge for understanding unconventional and/or high- T_c superconductors is elucidating how superconductivity emerges from adjacent phases whose interactions might foster [1–4] or inhibit [5, 6] electron pairing. Addressing this issue can be difficult, since often those phases—Mott insulator, spin or charge density wave, “strange metal,” and so on—are complex in their own rights. In this Letter, we perform angle-resolved photoemission spectroscopy (ARPES) *in situ* on thin films to reveal the electronic structure of BaBiO_3 , which is an insulating parent compound of superconductors with T_c exceeding 30 K upon doping. Our results indicate that BaBiO_3 is weakly correlated and characterized by a reverse (negative) Bi-O charge transfer, thus supporting a model in which hole pairs are condensed on combinations of the surrounding oxygen $2p$ orbitals [7]. The long-sought data are essential information for developing an understanding of the insulating state, its doping evolution, and superconductivity in bismuthates.

Figure 1(a) sketches the phase diagram of $\text{Ba}_{1-x}\text{K}_x\text{BiO}_3$ [8], which reaches the highest superconducting transition temperature among the bismuthates ($T_c^{\text{max}} = 32$ K). Pure BaBiO_3 is insulating to well above 800 K [9]. This electronic phase extends in an arc in the T -vs- x phase diagram out to $x \sim 0.3$. The insulating behavior is not only robust in terms of the high metal-insulator transition temperature and persis-

tence to high doping, but also with respect to multiple structural transitions within the insulating dome, which correspond to various degrees of breathing and tilting distortions of the BiO_6 octahedra. These distortions are depicted in Fig. 1(b) for the undoped system. The superconducting dome emerges with higher doping, with optimal T_c near $x = 0.38$. At relatively high doping and low temperature, the cubic metallic phase adopts a tetragonal structure en route to superconductivity.

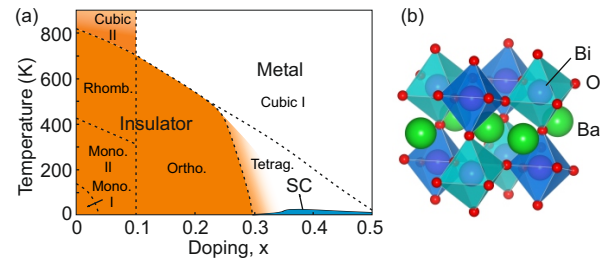


FIG. 1. (Color online) (a) Sketch of the x - T phase diagram of $\text{Ba}_{1-x}\text{K}_x\text{BiO}_3$. The space groups are: Mono. I = $P2_1/n$; Mono. II = $I2/m$; Rhomb. = $R\bar{3}$; Ortho. = $Ibmm$; Tetrag. = $I4/mcm$; Cubic I = $Pm\bar{3}m$; Cubic II = $Fm\bar{3}m$. (b) Depiction of the insulating ground state ($x = 0$) exhibiting breathing and tilting distortions. The collapsed and expanded BiO_6 octahedra are shown in dark blue and light blue (gray), respectively. In films, the tilting distortion is suppressed [10].

The origin and electronic nature of BaBiO₃'s insulating phase has been widely discussed. One would naively expect BaBiO₃ to be metallic with a half-filled 6s band, but the corresponding Bi⁴⁺ oxidation state is not found in nature. Thus the structure of alternating expanded and collapsed octahedra has often been interpreted as evidence of a corresponding charge-ordered state comprised of Bi³⁺ and Bi⁵⁺ sites [11]. However, with exceptions that we will later address [12, 13], experiments have not observed distinct bismuth valences in BaBiO₃ [14–20]. Some theories have modeled the insulating state in terms of an attractive (negative) effective on-site interaction, U [21, 22]. It has also been proposed that holes reside on the oxygen ligands [16, 20, 23], implying the influence of strong Bi-O hybridization or even a negative charge transfer energy. A recent computational study has advanced the negative charge transfer view, arguing that the split bands around E_F heavily derive from molecular-like combinations of O $2p$ orbitals while the Bi 6s states mostly contribute to dispersive bands located at deeper binding energy [7].

Given the questions raised about the role of (negative) effective on-site interactions in BaBiO₃, it is fair to ask whether single-electron models can accurately describe the band structure. Indeed, only recently have some calculations succeeded to obtain band gaps that match reasonably well with experiments [24]. Even then, the agreement between the calculated density of states (DOS) and momentum-integrated photoemission measurements remains underwhelming. An experimental determination of the band dispersions can provide better input for theorists and help judge the merits of various models.

ARPES is a powerful and direct probe of the electronic structure of solids in k space. Until now photoemission studies of BaBiO₃ have lacked momentum resolution [12, 15, 16, 19, 25, 26]. In order to obtain the ARPES data here, we overcame issues of charging and sample surface quality by growing smooth, crystalline thin films of BaBiO₃ on conducting, grounded bases and performing the experiments *in situ* on the freshly prepared samples. The measurements were performed at a sample temperature of 18–20 K. We compare the data with nonrelativistic density functional theory (DFT) calculations based on the local density approximation (LDA) using the low-temperature bulk space group $P2_1/n$. Additional details regarding the samples, measurements, and calculations can be found in the Supplemental Material [27].

The measured electronic structure is summarized in Fig. 2. We describe the momentum space in terms of k_z perpendicular to the (001) sample surface and orthogonal k_x and k_y momenta lying in the surface plane along the (100) and (010) cubic axes. In ARPES, a given photon energy, $h\nu$, extracts photoelectrons from a sheet of k_z values scanned in the k_x - k_y plane [28]. From detailed $h\nu$ -dependent scans, we verified that the observed electronic structure is three dimensional [27]. As illustrated

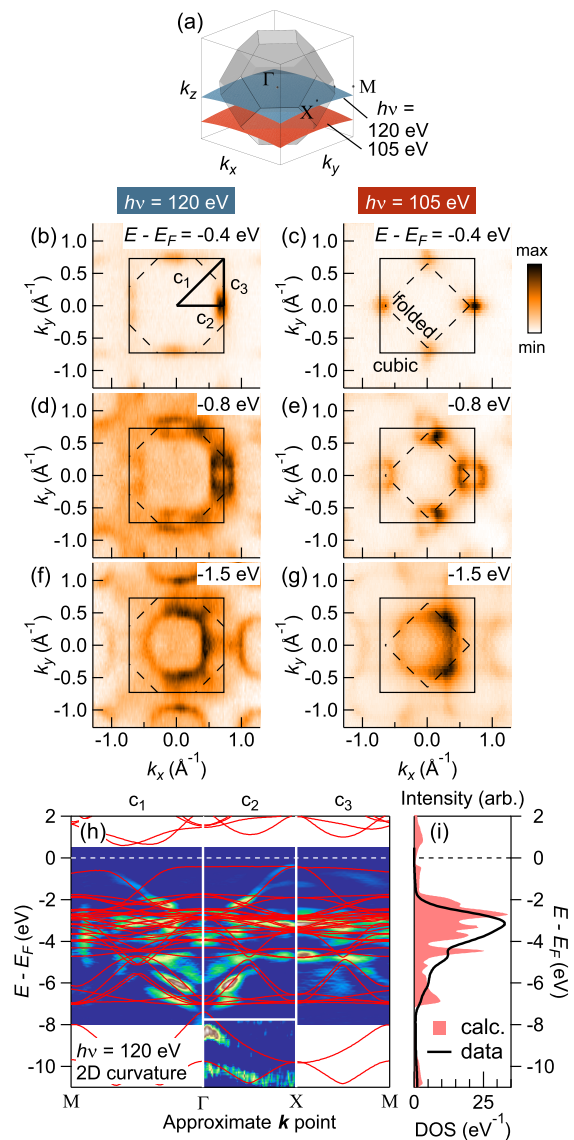


FIG. 2. (Color online) (a) Folded Brillouin zone due to breathing distortions of insulating BaBiO₃. The curved planes show the k_z values accessed by ARPES when using photon energies of 120 eV and 105 eV. (b)–(g) Left column: ARPES constant energy maps acquired using 120 eV photons, evaluated at $E - E_F = -0.4$, -0.8 , and -1.5 eV; Right column: Analogous maps acquired with $h\nu = 105$ eV. (h) Band dispersions along cuts c_1 , c_2 , and c_3 indicated in (b). The data have been analyzed using the 2D curvature method. LDA calculations of the band structure are overlaid on each cut. (i) Angle-integrated photoelectron intensity along cut c_2 (line) and calculated DOS (shading).

in Fig. 2(a), measurements performed with $h\nu = 120$ eV acquire data with k_z near the Γ point of the 3D Brillouin zone, while $h\nu = 105$ eV corresponds to a sheet located close to $k_z = -\pi/2a$, where a is the simple cubic lattice constant (≈ 4.3 Å). Figures 2(b)–2(g) show constant energy maps acquired with $h\nu = 120$ eV (left column) and

105 eV (right column) and evaluated at three different binding energies within the highest occupied bands. In all maps, the counts were integrated within a range of ± 15 meV.

The constant energy maps show that the symmetry of the electronic structure of the thin film samples is consistent with Brillouin zone folding as depicted in Fig. 2(a), which arises from oxygen breathing distortions. The different k_z values associated with the two photon energies lead to distinct appearances of the zone folding when viewed in the k_x - k_y plane. Namely, the in-plane projection of the folded Brillouin zone goes from being octagonal for $h\nu = 120$ eV to square in the case of $h\nu = 105$ eV. These projections are overlaid on their respective maps (dashed lines), along with the simple cubic Brillouin zone (solid lines).

Analysis of the band dispersions is presented in Fig. 2(h). Labels c_1 - c_3 refer to cuts through the data as marked in Fig. 2(b). To clarify the bands, the spectra have been processed using the 2D curvature method [29]. The \mathbf{k} -integrated intensity obtained from cut c_2 is shown in Fig. 2(i). LDA calculations of the bands and DOS are overlaid on the experimental data in Figs. 2(h) and 2(i), respectively. For the calculations, we eliminated the octahedral tilting distortion in accordance with the structure of BaBiO₃ thin films grown on various substrates [10]. This slightly increases the bandwidths and alters some band splittings, modestly but noticeably improving the agreement between the data and LDA. One should note that the *breathing* distortions still present in films are found to be the deciding structural factor in BaBiO₃'s insulating behavior [7, 10, 30]. Hence the general conclusions of the present study are believed to be applicable to bulk BaBiO₃.

The level of agreement between the data and calculations demonstrates that LDA methods can successfully compute most aspects of the band structure of BaBiO₃, including the bandwidths. Consequently, we can infer that electron correlations are weak. Certain portions of the calculated electronic structure, such as the flat band crossing Γ near E_F , are difficult to observe in the experiments. These features tend to be associated with a secondary folding, in addition to that of the breathing distortions, occurring in the low-temperature ‘‘Mono. I’’ $P2_1/n$ space group [Fig. 1(a)]. Ostensibly the symmetry-breaking potential associated with this secondary folding is weak, leading to the very low spectral weight of these features in ARPES [27]. Aside from that, the disagreements are quantitative and relatively minor, although the LDA tends to underestimate the band gap. Here the calculated direct gap is 1.45 eV, compared to an experimental value of ~ 2 eV in both bulk and thin film samples [31, 32]. Moreover, the calculation finds the indirect gap on the verge of closing, whereas our experiments show this is not the case [27]. More costly hybrid functionals might be able to obtain better quantitative results

regarding the band gap [24].

Photoemission spectroscopy from core levels is in principle well suited to address the issue of formal Bi charge ordering in BaBiO₃, but previous studies did not arrive at a consensus. Several measurements found little evidence of distinct Bi valence states [15, 16, 19, 25]; however, the outcomes were sensitive to the sample surface preparations, and in some cases additional peaks or shoulders were observed [12, 13, 33]. Because of the very short probing depth of photoemission techniques, it has not been clear which of these measurements—if any—represent the intrinsic bulklike electronic structure rather than some extrinsic and/or surface-related system that was perhaps contaminated, damaged, or structurally distorted.

Having demonstrated the 3D insulating band structure of the BaBiO₃ films, which matches well with calculations, the present experiments allow us to definitively assess the Bi core level spectra relevant to the bulklike electronic structure. Figure 3 shows the Bi 4*f* spectrum acquired with $h\nu = 220$ eV. No evidence of two distinct Bi charge states is seen; rather, the $j = 5/2, 7/2$ doublet is well fit by a double-Gaussian function. The peaks from BaBiO₃ are sharp in comparison to published data from Bi₂O₃ [25] and NaBiO₃ [13] (nominal representatives of pure Bi³⁺ and Bi⁵⁺ valence states, respectively), which argues against mixed or fluctuating valence of the Bi atoms.

To further uncover the electronic nature of BaBiO₃ and understand why bismuth charge ordering is not observed, we turn attention to the orbital compositions of the bands. Figure 4(a) shows the total and orbital-projected DOS computed from the band structure in Fig. 2(h). The calculations find that the highest occupied bands derive overwhelmingly from O 2*p* states, while most of Bi 6*s* states contribute to dispersive bands roughly 8 to 13 eV below E_F , accounting for the majority of the DOS in that energy range. These deep-energy bands, which are nearly

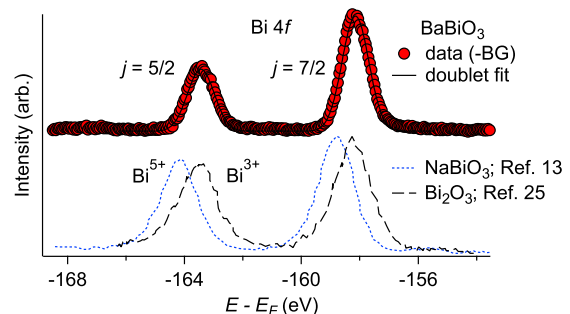


FIG. 3. (Color online) Bi 4*f* core level spectrum. Following background subtraction ($-BG$), the data (circles) are fit by two Gaussians (line). Spectra from Bi₂O₃ (dashed line; Ref. [25]) and NaBiO₃ (dotted line; Ref. [13]), representing cases of pure Bi³⁺ and Bi⁵⁺ valence states, respectively, are shown for comparison.

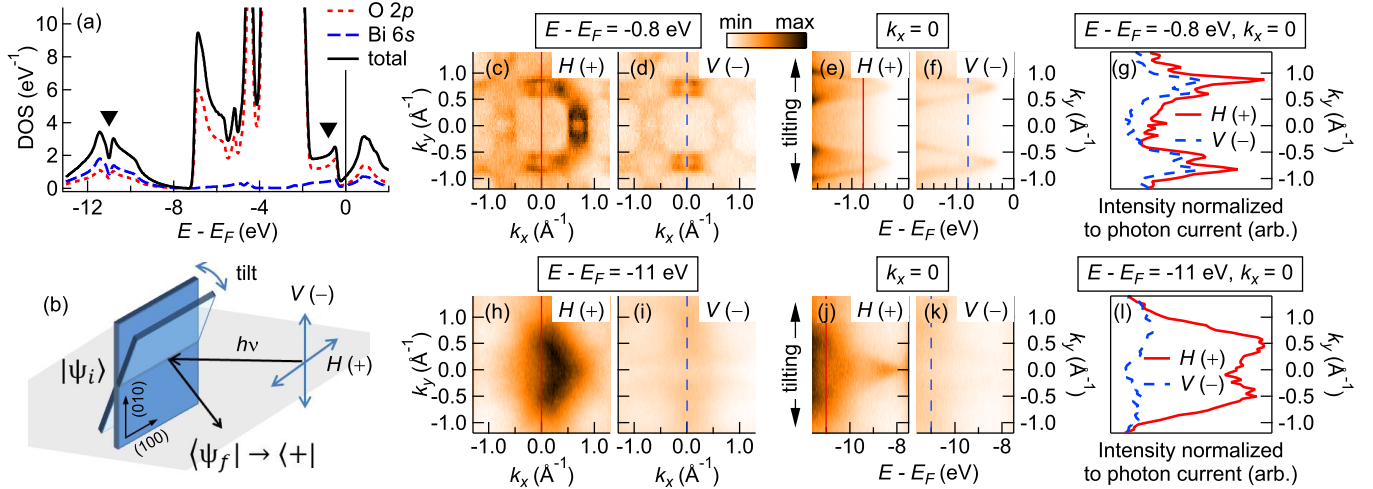


FIG. 4. (Color online) (a) Calculated total DOS (solid line), as well as the O 2*p* and Bi 6*s* orbital-projected DOS (short and long dashed lines, respectively). (b) Sketch of the experimental geometry. (c), (d) Constant energy maps at $E - E_F = -0.8$ eV acquired using $h\nu = 120$ eV with *H* and *V* photon polarizations. (e), (f) Near- E_F dispersion cuts through $k_x = 0$ acquired with *H* and *V* polarizations. The momentum k_y was varied by tilting the sample. (g) MDCs at $k_x = 0$ and $E - E_F = -0.8$ eV obtained with *H* and *V* polarizations (solid and dashed lines, respectively). The intensities have been normalized to the incident photon current of each polarization and shifted by an overall background offset. (h)–(l) Analogous to (c)–(g), except analyzed at deeper binding energies, as indicated.

invisible in momentum-integrated photoemission, can be unambiguously identified in the ARPES data [compare Figs. 2(h) and 2(i)]. This allows us to probe the photoemission matrix elements of these bands in order to check consistency with the calculated orbital hierarchy.

In our experimental geometry [Fig. 4(b)], the photoexcitation operator, $\mathbf{A} \cdot \mathbf{p}$, has even parity (+) with respect to the beam-detector plane when the radiation is horizontally (*H*) polarized and odd parity (−) for vertical (*V*) polarization. Regarding the detected photoelectron final state as a plane wave [28], the use of *V* polarized photons will cause the matrix element $M_{fi} \propto \langle \psi_f | \mathbf{A} \cdot \mathbf{p} | \psi_i \rangle^2$ to vanish when the initial state is even (i.e., $M_{fi} \rightarrow \langle + | - | + \rangle^2 = 0$). By contrast, the same state would generally be visible when probed in the *H* polarization mode. Thus, as a telling signature, a majority *s*-orbital character band should exhibit strong tilt-independent suppression of the photoemission intensity upon switching from *H* to *V* polarization. A band composed of combinations of *p* orbitals, on the other hand, would display more complicated tilt-dependent intensity differences between the two polarization modes, since the orbitals' parities depend on the geometry.

As shown in Figs. 4(c) and 4(d), constant energy maps at $E - E_F = -0.8$ eV acquired with *H* polarization are similar to those obtained using *V* polarization, simply differing in their intensity modulations as a function of the geometry. In dispersion cuts at $k_x = 0$, which are obtained by tilting the sample, the highest occupied band is clearly visible over its full bandwidth for both incoming polarizations [Figs. 4(e) and 4(f)]. The peak features

seen in momentum distribution curves (MDCs) evaluated at $E - E_F = -0.8$ eV and $k_x = 0$, shown in Fig. 4(g), have similar intensities for both polarizations. The behavior is markedly different at deeper binding energies of $E - E_F \lesssim -8$ eV, where the features seen in the *H* mode nearly vanish when probed with *V* polarization [Figs. 4(h)–4(l)]. The strong tilt-independent suppression of spectral weight observed from the bands at deep binding energy is consistent with a majority *s*-orbital character and serves as further validation of the LDA-computed DOS.

The determined orbital hierarchy, in which O 2*p* states dominate at the gap edge and the Bi 6*s* states are concentrated far below E_F , indicates that holes in BaBiO₃ reside primarily on the oxygen orbitals. This, in turn, provides an explanation for the lack of bismuth charge ordering: hole pairs from the would-be Bi⁵⁺ sites of the collapsed octahedra are transferred to the oxygen ligands, leaving behind just Bi³⁺, consistent with core level measurements (Fig. 3). LDA calculations of closely related SrBiO₃ found that these holes specifically occupy A_{1g} combinations of the O 2*p* orbitals within the sublattice of collapsed BiO₆ octahedra [7]. We note that the resulting electronic configuration resembles an *s*-*p* analog of a model proposed for nickelates [34–37].

The overall agreement between the measured and calculated band structure builds confidence in conclusions drawn from DFT studies. One clear implication is that strong nesting of the underlying Fermi surface of cubic BaBiO₃ leads to a large static susceptibility peaked at $Q = (\pi, \pi, \pi)/a$ [7, 38, 39]. The charge density wave

state in BaBiO₃ is remarkable, however, in terms of its fully gapped 3D band structure and its temperature and doping stability. These properties might derive in part from influences beyond a pure Peierls model. Specifically, added holes have been proposed to form trapped (bi)polarons inside the gap [40], which is likewise supported by the application of DFT [41].

These and other studies [42] certainly point toward strong electron-phonon interactions in BaBiO₃, although it is still not clear whether the high optimal T_c in, e.g., Ba_{1-x}K_xBiO₃ can be entirely explained within BCS strong coupling theory [43, 44]. For example, as (bi)polarons become mobile with increased hole doping, superconductivity in the bismuthates could involve *local* bosonic pairs [45, 46]. In many cases, bipolaronic superconductivity has been discussed in the context of a classically charge-ordered state in BaBiO₃, regarding electron and hole pairs as localized on the supposed Bi³⁺ and Bi⁵⁺ sites. Our data demonstrate that in the undoped ground state *all* Bi atoms have essentially filled 6s shells, and the Bi sites of the collapsed and expanded octahedral sublattices differ in terms of their screening by holes distributed on the surrounding oxygen orbitals. Theories of superconductivity in bismuthates (bipolaronic or otherwise) may benefit from taking this more accurate description of the electronic configuration and screening into account.

In conclusion, by performing *in situ* spectroscopy on freshly grown films, we have obtained the first ARPES measurements from the high- T_c parent compound BaBiO₃. The data are in good agreement with DFT-LDA calculations. The simultaneous observations of the folded Brillouin zone due to oxygen breathing distortions and sharp, single-component Bi core levels demonstrate that the structurally inequivalent Bi sites have virtually identical valences. In the calculations, the bands closest to E_F are primarily derived from O $2p$ states, while the Bi $6s$ states mostly contribute to the deep-energy band structure, which is shown to be consistent with the behavior of the ARPES matrix elements. The results signal the influence of a negative charge transfer energy, driving hole pairs to occupy ligand states on the collapsed octahedra. The findings should be relevant for understanding the doping evolution and superconducting behavior of doped bismuthate compounds.

* nicholas.plumb@psi.ch

† On leave from Institute of Physics, Polish Academy of Sciences, Aleja Lotnikow 32/46, PL-02-668 Warsaw, Poland

- [1] P. W. Anderson, *Science* **235**, 1196 (1987).
 [2] D. J. Scalapino, *Phys. Rep.* **250**, 329 (1995).
 [3] M. T. Béal-Monod, C. Bourbonnais, and V. J. Emery, *Phys. Rev. B* **34**, 7716 (1986).
 [4] I. Mazin and J. Schmalian, *Physica C* **469**, 614 (2009).
 [5] J. Chang *et al.*, *Nature Phys.* **8**, 871 (2012).
 [6] G. Ghiringhelli *et al.*, *Science* **337**, 821 (2012).
 [7] K. Foyevtsova *et al.*, *Phys. Rev. B* **91**, 121114 (2015).
 [8] A. W. Sleight, *Physica C* **514**, 152 (2015).
 [9] F. Munakata, A. Nozaki, T. Kawano, and H. Yamauchi, *Solid State Commun.* **83**, 355 (1992).
 [10] K. Inumaru, H. Miyata, and S. Yamanaka, *Phys. Rev. B* **78**, 132507 (2008).
 [11] D. Cox and A. Sleight, *Solid State Commun.* **19**, 969 (1976).
 [12] Y. Jeon *et al.*, *Phys. Rev. B* **41**, 4066 (1990).
 [13] G. U. Kulkarni *et al.*, *Appl. Phys. Lett.* **57**, 1823 (1990).
 [14] J. de Hair and G. Blasse, *Solid State Commun.* **12**, 727 (1973).
 [15] G. K. Wertheim, J. P. Remeika, and D. N. E. Buchanan, *Phys. Rev. B* **26**, 2120 (1982).
 [16] Z.-X. Shen *et al.*, *AIP Conf. Proc.* **200**, 30 (1990).
 [17] J. B. Boyce *et al.*, *Phys. Rev. B* **41**, 6306 (1990).
 [18] Z. N. Akhtar, M. J. Akhtar, and C. R. A. Catlow, *J. Phys.: Condens. Matter* **5**, 2643 (1993).
 [19] H. Namatame *et al.*, *Phys. Rev. B* **50**, 13674 (1994).
 [20] A. Ignatov, A. Menushenkov, and V. Chernov, *Physica C* **271**, 32 (1996).
 [21] T. M. Rice and L. Sneddon, *Phys. Rev. Lett.* **47**, 689 (1981).
 [22] C. M. Varma, *Phys. Rev. Lett.* **61**, 2713 (1988).
 [23] A. P. Menushenkov and K. V. Klementev, *J. Phys.: Condens. Matter* **12**, 3767 (2000).
 [24] C. Franchini *et al.*, *Phys. Rev. B* **81**, 085213 (2010).
 [25] M. S. Hegde *et al.*, *Phys. Rev. B* **39**, 4752 (1989).
 [26] R. Itti *et al.*, *Phys. Rev. B* **43**, 435 (1991).
 [27] See Supplemental Material at <http://link.aps.org/supplemental/10.1103/PhysRevLett.117.037002>, which includes Refs. [10, 28, 29, 47–58], and contains further details about the samples, preparation techniques, measurements, and data analysis.
 [28] A. Damascelli, *Phys. Scr.* **T109**, 61 (2004).
 [29] P. Zhang *et al.*, *Rev. Sci. Instrum.* **82**, 043712 (2011).
 [30] T. Thonhauser and K. M. Rabe, *Phys. Rev. B* **73**, 212106 (2006).
 [31] S. Tajima *et al.*, *Phys. Rev. B* **32**, 6302 (1985).
 [32] H. Sato *et al.*, *Nature (London)* **338**, 241 (1989).
 [33] M. Nagoshi *et al.*, *J. Phys.: Condens. Matter* **4**, 5769 (1992).
 [34] T. Mizokawa, D. I. Khomskii, and G. A. Sawatzky, *Phys. Rev. B* **61**, 11263 (2000).
 [35] H. Park, A. J. Millis, and C. A. Marianetti, *Phys. Rev. Lett.* **109**, 156402 (2012).
 [36] B. Lau and A. J. Millis, *Phys. Rev. Lett.* **110**, 126404 (2013).
 [37] S. Johnston *et al.*, *Phys. Rev. Lett.* **112**, 106404 (2014).
 [38] L. F. Mattheiss and D. R. Hamann, *Phys. Rev. B* **28**, 4227 (1983).
 [39] S. Sahrakorpi *et al.*, *Phys. Rev. B* **61**, 7388 (2000).
 [40] I. B. Bischofs, V. N. Kostur, and P. B. Allen, *Phys. Rev. B* **65**, 115112 (2002).
 [41] C. Franchini, G. Kresse, and R. Podloucky, *Phys. Rev. Lett.* **102**, 256402 (2009).
 [42] G.-m. Zhao *et al.*, *Phys. Rev. B* **62**, R11977 (2000).
 [43] T. Bazhiron *et al.*, *Phys. Rev. B* **88**, 224509 (2013).
 [44] Z. P. Yin, A. Kutepov, and G. Kotliar, *Phys. Rev. X* **3**, 021011 (2013).
 [45] R. Micnas, J. Ranninger, and S. Robaszkiewicz, *Rev.*

- Mod. Phys. **62**, 113 (1990).
- [46] N. Mott, *Physica A* **200**, 127 (1993).
 - [47] H. M. Rietveld, *J. Appl. Crystallogr.* **2**, 65 (1969).
 - [48] J. Rodríguez-Carvajal, *Physica B* **192**, 55 (1993).
 - [49] S. Pei *et al.*, *Phys. Rev. B* **41**, 4126 (1990).
 - [50] B. M. Moon *et al.*, *Appl. Phys. Lett.* **59**, 1905 (1991).
 - [51] D. P. Norton *et al.*, *Appl. Phys. Lett.* **62**, 414 (1993).
 - [52] D. Mijatovic *et al.*, *Physica C* **372–376**, 596 (2002).
 - [53] G. Kim *et al.*, *Phys. Rev. Lett.* **115**, 226402 (2015).
 - [54] H. Uwe and K. Tachibana, in *Advances in Superconductivity VII*, edited by K. Yamafuji and T. Morishita (Springer Japan, 1995) pp. 165–168.
 - [55] D. A. Shirley, *Phys. Rev. B* **5**, 4709 (1972).
 - [56] P. Giannozzi *et al.*, *J. Phys.: Condens. Matter* **21**, 395502 (19pp) (2009).
 - [57] J. P. Perdew and A. Zunger, *Phys. Rev. B* **23**, 5048 (1981).
 - [58] B. J. Kennedy *et al.*, *Acta Crystallogr. Sect. B* **62**, 537 (2006).

The authors thank G. A. Sawatzky, K. Foyevtsova, and C. Mudry for insightful discussions. F. Dubi, M. Kropf, and L. Nue provided technical assistance at SIS beam line. D. J. G. received financial support from Sciex-NMSch (Project No. 13.236) funded by the Swiss Confederation. Y. W. and S. J. were supported by the University of Tennessee’s Science Alliance Joint Directed Research and Development (JDRD) program, a collaboration with Oak Ridge National Laboratory. S. J. acknowledges additional support from the University of Tennessee’s Office of Research & Engagement’s Organized Research Unit program. CPU time was provided in part by resources supported by the University of Tennessee and Oak Ridge National Laboratory Joint Institute for Computational Sciences (<http://www.jics.utk.edu>).